PAPER • OPEN ACCESS

Plastic and superionic phases in ammonia–water mixtures at high pressures and temperatures

To cite this article: Victor Naden Robinson and Andreas Hermann 2020 *J. Phys.: Condens. Matter* **32** 184004

View the article online for updates and enhancements.

IOP ebooks™

Bringing you innovative digital publishing with leading voices to create your essential collection of books in STEM research.

Start exploring the collection - download the first chapter of every title for free.

Plastic and superionic phases in ammonia–water mixtures at high pressures and temperatures

Victor Naden Robinson[1,2] and Andreas Hermann[1]

[1] Centre for Science at Extreme Conditions and SUPA, School of Physics and Astronomy, University of Edinburgh, Edinburgh, EH9 3FD, United Kingdom
[2] The Abdus Salam International Centre for Theoretical Physics (ICTP), Trieste, Strada Costiera 11, 34151, Italy

E-mail: a.hermann@ed.ac.uk

CrossMark

Abstract

The interiors of giant icy planets depend on the properties of hot, dense mixtures of the molecular ices water, ammonia, and methane. Here, we discuss results from first-principles molecular dynamics simulations up to 500 GPa and 7000 K for four different ammonia–water mixtures that correspond to the stable stoichiometries found in solid ammonia hydrates. We show that all mixtures support the formation of plastic and superionic phases at elevated pressures and temperatures, before eventually melting into molecular or ionic liquids. All mixtures' melting lines are found to be close to the isentropes of Uranus and Neptune. Through local structure analyses we trace and compare the evolution of chemical composition and longevity of chemical species across the thermally activated states. Under specific conditions we find that protons can be less mobile in the fluid state than in the (colder, solid) superionic regime.

S Supplementary material for this article is available online

(Some figures may appear in colour only in the online journal)

1. Introduction

The 'ice giants' Uranus and Neptune have gaseous atmospheres (rich in hydrogen and helium) and small rocky cores but they are dominated by their vast mantle regions, which comprise mixtures of the 'molecular ices' water, ammonia and methane. These same mixtures are presumed to feature prominently in the large number of Neptune-like exoplanets discovered by recent and current astronomical observation campaigns [1–7]. They are exposed to a wide range of pressure and temperature conditions. There is some ambiguity about how molecular ices organize themselves inside these planetary bodies—e.g. as segregated layers with distinct chemical and density profiles, or as quasi-homogeneous mixtures mirroring essentially the global composition ratio. The low luminosity of Uranus could be explained by the presence of a thermal boundary layer in its mantle region [8, 9], which would suggest quite drastic composition gradients in its interior. In general, high-pressure conditions up to hundreds of GPa inside ice giants can favor unexpected chemical motifs, and stabilize unusual compounds and stoichiometries. This has been shown for prototypical mineral compounds [10–14], individual planetary ices [15–21], and lately also for their mixtures [22–26].

Mixtures of ammonia and water are of particular interest in this context as they can form nearly or completely hydrogen-bonded networks in the solid state. Their

hydrogen bonds N–H $\cdots$ O and O–H $\cdots$ N mirror those seen in DNA and RNA and proteins in general, and it is of interest to understand their reaction to external compression as one limiting factor of life under extreme conditions. Three stoichiometric ammonia hydrates exist in nature and have been explored around ambient and low-pressure conditions: ammonia monohydrate (AMH, $NH_3:H_2O = 1:1$), ammonia dihydrate (ADH, 1:2) and ammonia hemihydrate (AHH, 2:1) [27, 28]. For comparison, the ammonia:water solar abundance ratio is 1:7 [29]. The three hydrates' phase diagrams show appreciable complexity: at various $P − T$ conditions, five solid AMH and ADH phases, as well as three solid AHH phases have been identified in experiment, even though some of their structures have not been resolved. There are known relations between the three mixtures: both ADH and AMH decompose into AHH and ice-VII, around 3 GPa and at 280 K and 250 K, respectively, while ADH also decomposes into AMH and ice-VII around 0.55 GPa and 190 K [30, 31]. Moreover, around 5–20 GPa and room temperature, *all* ammonia hydrates are found to form disordered molecular alloy (DMA) phases, with substitutional disorder of ammonia and water on a body-centered cubic (bcc) lattice; meanwhile, calculations predict partial ionization into OH^- and NH_4^+ in all hydrates [23, 30, 32–34]. The AHH-DMA phase has been observed in two independent experiments [34, 35] that found, at low temperatures, transitions from AHH-II to AHH-DMA at 19–30 GPa. The AHH-DMA phase was found to remain stable up to the highest experimental pressure studied, 41 GPa [34].

A series of recent computational studies has explored the ground states of ammonia–water mixtures to higher pressures using crystal structure prediction methods [24, 25, 36, 37]. Some studies are restricted to specific compounds, AMH [36] and ADH [37], and also explored the high-temperature regime using *ab initio* molecular dynamics (AIMD) simulations. These focused in particular on the appearance of superionicity—states characterized by diffusive protons in otherwise solid lattices of heavy nuclei [38]—but also the melting line. However, more recent studies reported more stable high-pressure phases of AMH and ADH, and also established the phase relations in the full ammonia–water composition space. This resulted for instance in the suggestion of a fourth ammonia hydrate, an ammonia-rich 4:1 mixture called AQH, to become stable around 25 GPa and remain thus up to 2–3 Mbar [24, 25].

In the present work, we use AIMD simulations to explore the high-pressure/high-temperature regime of *all* known ammonia–water mixtures, in each case starting from the most relevant high-pressure solid phases and investigating temperature-induced phase changes. Both NH_3 and H_2O are reported to feature 'plastic' phases, where individual molecules become free rotors but remain affixed to a solid lattice [39–42]. The presence of such phases has not been considered for mixtures of ices so far. Upon further heating compressed planetary ices are expected to transition into superionic regimes and eventually melt. It is of particular interest whether the melting line intersects the isentropes of Uranus or Neptune, which would

suggest a partially solid lower mantle in these planets that retains efficient electrical and thermal conductivity through proton transport. This phase evolution has been reported for the individual ices of NH_3 and H_2O [16, 41, 43–46], for mixtures of helium and water [47], ternary mixtures including methane [48] and, as already mentioned, has also been calculated for AMH and ADH [36, 37].

We show here that plasticity and superionicity are general features of all ammonia water mixtures under pressure; that their melting lines are close to the isentropes of Uranus and Neptune; and provide detailed analyses of the chemical composition of the mixtures at high $P − T$ conditions.

2. Computational methodology

Density functional theory (DFT) calculations were performed with the CASTEP code [49]. Exchange-correlation effects were described within the generalized gradient approximation (GGA) using the Perdew–Burke–Ernzerhof (PBE) functional [50] and ultrasoft pseudopotentials. Previous work on the high-pressure ground state phase diagrams of these compounds showed little influence of the choice of exchange-correlation functional [25]. Final structure relaxations were done with 'hard' pseudopotentials with cutoff radii no greater than 1.2 Å for oxygen and nitrogen, and 0.6 Å for hydrogen. Plane-wave cutoffs of $E_c = 1000$ eV, reduced to 700 eV for AIMD, and k-point densities of 20/Å^{-1} were found to give sufficiently converged energies and forces. AIMD used the Γ-point in the Brillouin zone only, a time-step of 0.5 fs and the NVT ensemble where the pressure was sampled every 10 time steps. Solid phases were compared at finite temperatures by obtaining free energies from vibrational entropy calculations within the harmonic approximation. The Gibbs free energy as a function of temperature for a solid is given by $G(T) = E + PV + E_{ZPE} + \int \frac{\hbar\omega}{\exp(\frac{\hbar\omega}{k_B T}-1)} F(\omega)\, d\omega$, where E_{ZPE} is the zero point energy given by $E_{ZPE} = \frac{1}{2} \int F(\omega)\hbar\omega\, d\omega$, and $F(\omega)$ is the phonon density of states, obtained from suitable supercell calculations.

We performed AIMD simulation on the four mixtures that are found to be stable in the ground state: ADH, AMH, AHH, and AQH. For each mixture, a regular grid of density-temperature points was investigated, covering their respective range of stability, and starting from the most stable crystal structure at any given pressure. MD trajectories were analysed through radial and partial distribution functions, mean squared displacements (MSD), local bond connectivity, and O–H and N–H covalent bond life times. Deduced properties include diffusion coefficients, classification of different states (as plastic/locally excited, superionic, or fluid), the melting lines, local characteristics of the fluid, and presence of various chemical species. In total, 1.528 ns of AIMD trajectories were accumulated and analysed.

We determined bond life times by firstly calculating a bond auto correlation function (BAC). The BAC, $\beta(t)$, measures the probability of a specific bond between two atoms i and j present at time t_0 to exist at a later time $t_0 + t$. Specifically,

$$\beta(t) = \left\langle \frac{b_{ij}(t_0) \cdot b_{ij}(t_0 + t)}{b_{ij}(t_0)^2} \right\rangle \qquad (1)$$

where $b_{ij}(t_0) = 1$ if a bond between atoms i and j exists at time t_0, and $b_{ij}(t_0) = 0$ otherwise. If all bonds remain stable throughout the simulation, $\beta(t)$ should tend to unity, and otherwise decay with a characteristic time constant τ that can be associated with the bond life time. $\beta(t)$ as defined uses information from persistent bonds that do not easily break during a typical simulation run.

3. Results

3.1. AIMD phase diagrams

The $P - T$ phase space for each mixture to be covered by AIMD was based on their low temperature stability established in previous works [24, 25] and up to at least $T = 5000$ K. For example, the most stable high pressure mixture, AHH, was considered up to 500 GPa and 7000 K. The resulting phase diagrams are shown in figure 1. For reference, these also include data from previous AIMD studies on AMH and ADH [36, 37] and estimates for the isentropes of Neptune and Uranus [51]. Solid–solid phase boundaries are constructed from free energies that include vibrational entropy effects at the harmonic level. For all mixtures, we identify regions of solid phases, rotating or plastic phases, superionic phases, and finally liquid phases. These states were classified by inspecting the MSD as illustrated in figure 2. The plastic or locally excited regime has a finite MSD for protons that plateaus at small values. The superionic regime has diffusive protons and finite proton diffusion constants $D_H > 0$ while maintaining a solid heavy atom lattice ($D_N = D_O = 0$). Finally, in the molten state, all atoms are fully mobile and diffuse through the simulation boxes.

For the different mixtures, we can make some general observations from their respective $P - T$ phase diagrams. The properties of the different high-temperature phases (featuring local excitations, plasticity and superionicity, and eventual melting) are discussed in detail in subsequent subsections.

The solid phases of AHH were simulated up to 500 GPa, which covers the pressure region where AHH is stable among the water–ammonia mixtures; it should decompose into the elemental ices above 460 GPa at low temperatures. Every AHH phase entered an excited or plastic regime upon heating, before either melting directly (at very low pressures) or becoming superionic and then eventually melting at much higher temperatures. Between 200 and 300 GPa the excited regime extends beyond 1500 K, higher than seen in any other mixture. The melting line crosses the isentropes of Uranus and Neptune at intermediate pressures (indicating a superionic region of mixed ices inside these planets is possible) but appears to flatten out above 300 GPa, to the extent that the innermost mantle regions could be fully liquid.

In AQH the phase diagram includes simulations of all solid phases up to 300 GPa. Again most phases (those above 60 GPa) enter an excited region at 1000 K and upon further heating the superionic regime before eventual melting. As an outlier, the low-pressure AQH-$P2_1$ phase exhibits excited behavior

at modest conditions of 500 K and 20 GPa. This phase is in the low pressure regime where AQH is not very stable and perhaps this allows for molecular units with weaker intermolecular interactions to be less tightly bound or for greater free volume within the unit cell, which in turn enable molecular rotations and temporary charge transfers (see details below). Above 100 GPa and 3000 K the melting line follows the isentropes of Uranus and Neptune very closely, possibly hinting at the presence of a superionic phase inside their mantles.

For ADH, simulations were chosen to have the same number of molecules (up to 432) as in the previous work by Jiang *et al* [37], to allow for comparable simulation conditions and to accommodate the unit cell of the large $I4_1cd$ phase (48 molecules per unit cell) relevant around 10 GPa. As Jiang *et al* reported superionic transitions at unusually low temperatures, a fine grid of PT simulation points was chosen to cover the range 100–1000 K for this mixture. Upon heating, molecular units were observed to rotate and at higher temperatures form superionic phases, as expected. In general, we find that the onset of superionicity reported by Jiang *et al* either corresponds to full melting (at 5 GPa) or the onset of plastic phases (10 GPa and above). AIMD simulations run for less than 2 ps must be interpreted carefully, as extrapolating the MSD trends can be misleading (see next subsection). Because of the presence of plastic phases we find the superionic transition for the $I4_1cd$ phase higher in temperature than Jiang *et al*, at 700–800 K. At higher pressures the $Ama2$ phase is found more stable than $I4_1cd$ [25], which has higher transition temperatures into the excited and superionic regions. For the high-pressure $P2_1/m$ phase no excited region was found but could occur between 1000 or 1500 K. These results partially agree with Jiang *et al* but differences stand out regarding details of the transition conditions, the nature of the thermally excited states and, due to more stable ground-state phases, shifts of temperature-induced phase changes to higher temperatures.

Simulations of AMH were performed in temperature increments of 500 K over a smaller pressure range than by Bethkenhagen *et al* [36], which accounts for the predicted decomposition of AMH into AHH and water above 1 Mbar [25]. Note that Bethkenhagen *et al* used 32 molecules per cell, while our simulations used 144–288 molecules per cell in each run and included different ground state structures beyond the $P4/nmm$ phase, i.e. above 40 GPa. Our results show different melting lines, onset of superionicity and, in our case, the emergence of locally excited phases across most of the pressure range. We detect melting in our simulations at temperatures that are mostly lower than those reported by Bethkenhagen *et al*, which can be reasoned through less superheating of solids in larger MD supercells. Note that our melting line does therefore not cross the Uranus and Neptune isentropes, a qualitative difference from previous reports. On the other hand, the present work used more stable solid phases such as $P4_3$, which should be harder to melt; it seems unlikely that the less enthalpically stable phases found in previous works would exhibit higher melting temperatures. An exception is the solid–superionic–liquid triple point that Bethkenhagen *et al* put around 20 GPa and 800 K. We find that the underlying solid phase ($P4/nmm$) is still superionic at 1000 K and
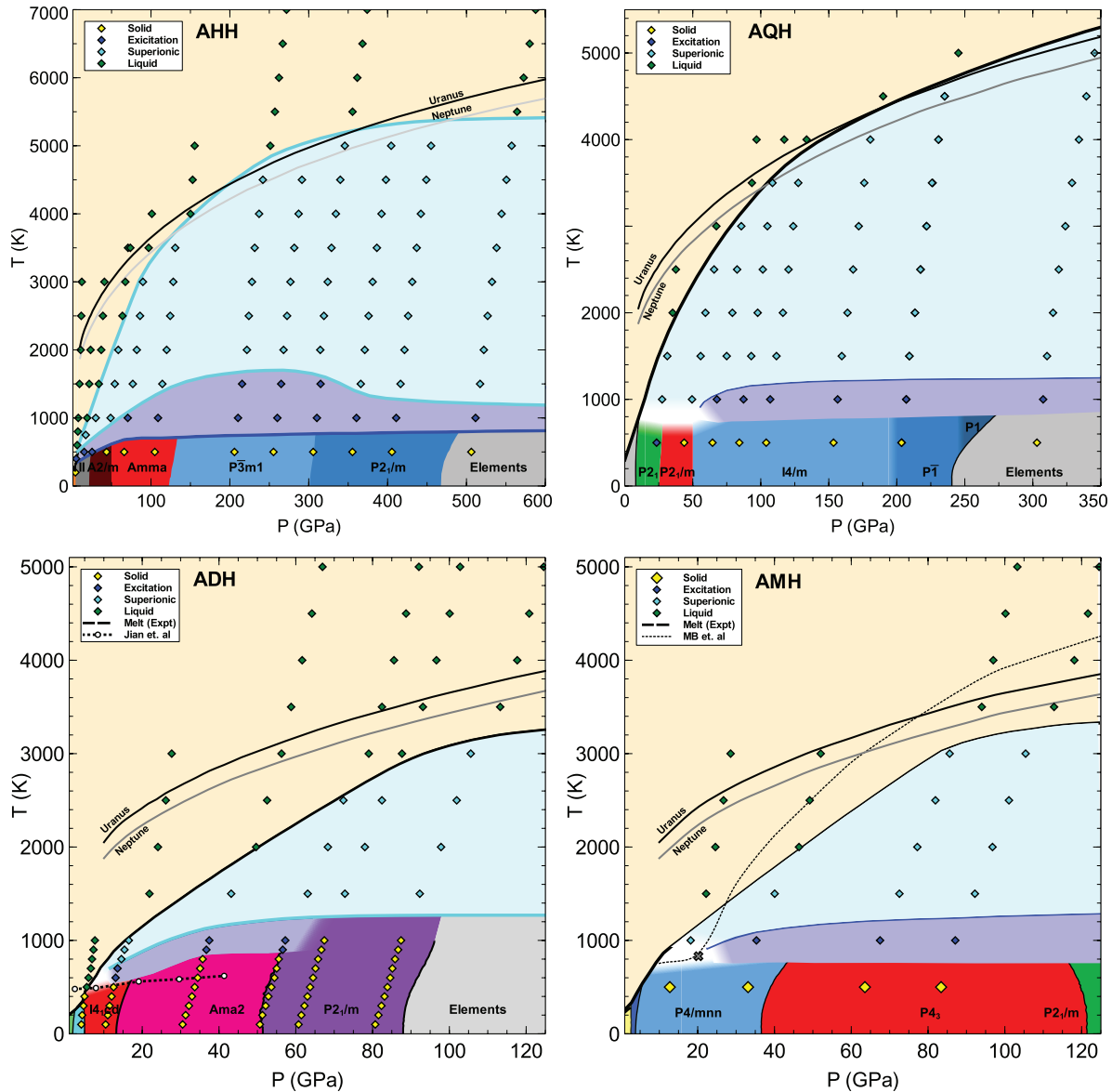
Figure 1. Phase diagrams for the four ammonia hydrates in their regions of stability. Dark blue shaded regions refer to plastic or locally excited phases. Cyan shaded regions are the superionic phases. Orange denotes the liquid, and solid phases are labelled and coloured individually. Experimental melt lines for ADH and AMH are from [34]. For AMH the grey cross notes the triple point from [48] and the dashed line represents the melt line from the same study. For ADH the dashed line with white circles represents the superionic transition line found in [37].

molten only at 1500 K. This discrepancy is interesting as more molecules were used in this study, which normally leads to more accurate (read: lower) melting temperatures, though the longer run-times afforded by using fewer molecules in previous works may have led to reaching the equilibrium state of the liquid at a lower temperature instead. Above 30 GPa and around 1000 K we find that AMH enters excited rotating phases (see figure 2) while superionicity is not observed until 1500 K.

3.2. Plasticity and local excitations

Plastic phases of molecular crystals refer to states which contain molecules that are free rotors but remain bound to their respective lattice sites. These phases have been identified at elevated temperatures and pressures in simulations of H_2O and NH_3, and seen in experiment for the latter [39–42]. Such phases are intermediates between the solid and fully liquid state. For mixtures of ices, the situation can be more complicated as there are many different structural and chemical motifs and sources of proton attraction, resulting in different types of local excitations—here defined as atoms departing from their lattice sites but not entering a diffusive state. Note that several molecular low pressure phases in AMH, ADH and AHH are configurationally proton-disordered, typically on the sites of NH_3 molecules that are least tightly bound into the overall hydrogen bonding network; this suggests that plasticity could also be a feature in these mixtures.

Indeed, in our simulations, we found that *all* mixtures entered a plastic regime under specific $P - T$ conditions,
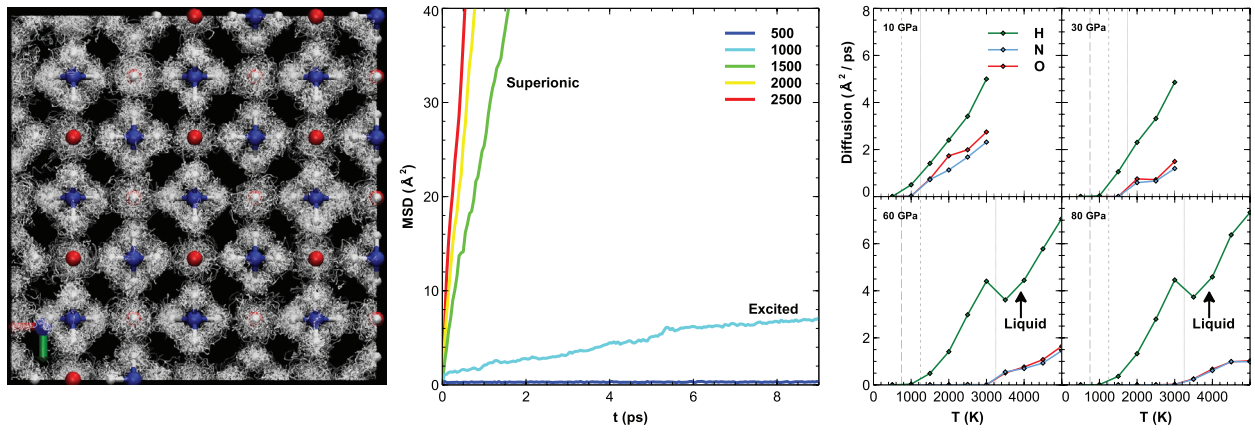
Figure 2. AIMD data for AMH. Left: typical trajectory for AMH-$P4/nmm$ at 30 GPa and 1000 K, with full proton trajectories over 10 ps run shown as white points (red/blue spheres are O/N positions). Middle: proton MSD for different temperatures at 30 GPa. Right: diffusion constants for the different atomic species as a function of temperature at four pressures. Long dash / short dashed / dotted lines denote onsets of excited / superionic / fluid regimes.
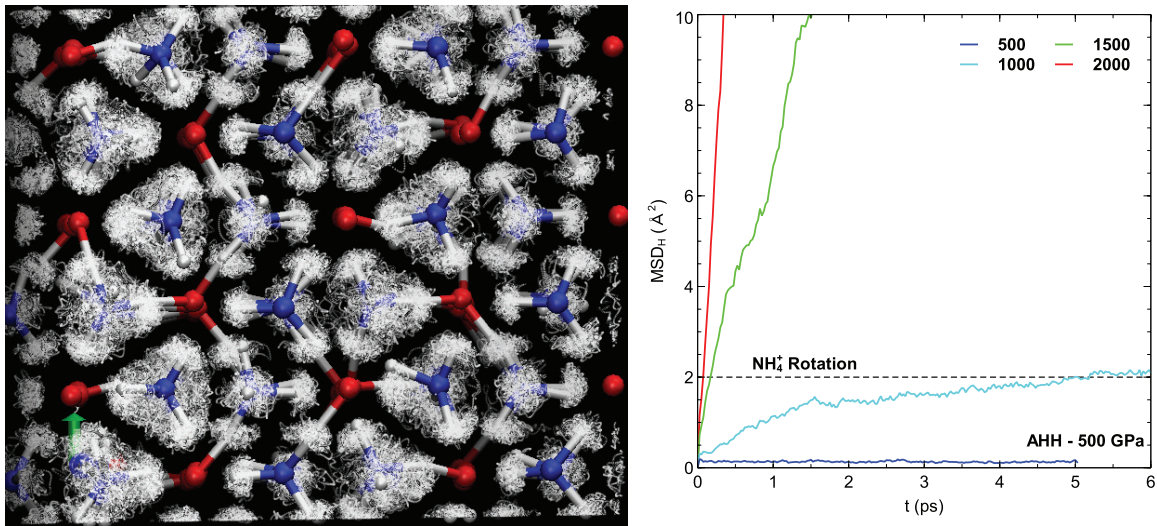

Figure 3. Left: AIMD trajectory of AHH-$P\bar{3}m1$ at 500 GPa and 1000 K with the full proton trajectory over 5 ps shown as white points. Bonds are drawn between N/O and protons with a cutoff distance of 1.1 Å for the final trajectory step. Right: proton MSD for AHH at 500 GPa and a large set of temperatures. Dashed line shows ideal MSD of freely rotating NH_4^+.

and these can be quite extreme. In figure 3 we show a typical MD trajectory for AHH at 500 GPa and 1000 K, displaying all proton positions. It is clear that protons are quite mobile but do not diffuse throughout the simulation cell. In fact, the dominant local excitations are rotations of NH_4^+ units as well as temporary proton donations along hydrogen bonds from NH_4^+ to O^{2-} anions, resulting in a dynamical equilibrium $NH_4^+ + O^{2-} \rightleftharpoons NH_3 + OH^-$. The proton MSD for this simulation, also shown in figure 3, appears to continually rise for 1.5 ps but then converges to a value around 2.0 Å^2. The distance between proton sites on the NH_4^+ unit in AHH-$P\bar{3}m1$ at 500 GPa is $d_{HH} = 1.625$ Å. Assuming the structure maintains the same local tetrahedral symmetry before and after molecular rotations the MSD should be expected to converge to $MSD_H = 3/4 \times d_{HH}^2 = 1.98$ Å^2 (protons are in their initial position for 1/4 of the time). This means there is a regime of finite values of MSD in simulating molecular compounds at extreme conditions that does not correspond to a (slow)

diffusive regime. For instance, in the work of Jiang *et al* [37] such plasticity may have been misinterpreted as superionicity.

From visually inspecting simulations at temperatures too low for superionicity but hot enough to feature excitations we can identify the different local excitations that are present, see figure 4: they involve rotations of neutral and ionic molecules, temporary proton hopping along hydrogen bonds, and occasional exchange of heavy atoms N and O—all occur in this regime before further heating creates a clearly superionic phase. All these events lead to finite proton MSD but with a vanishing slope (i.e. diffusion constant) at long simulation run time. For rotating molecules, the proton MSD should increase initially and then oscillate around a converged value where protons are halfway from their maximum displacement. Rotations can occur as quasi-free rotors, as in the plastic phases of pure H_2O and NH_3, or as jumps between different configurations with more-or-less linear hydrogen bonds. Proton hopping can occur as a temporary effect, for example
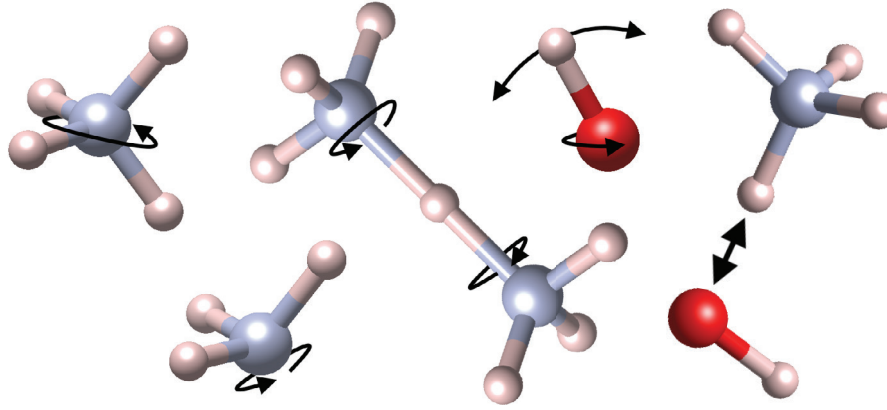
Figure 4. Example movements of the locally excited phases at temperatures below the superionic regime, visualizing rotational modes for various species and temporary proton transfer along hydrogen bonds.

in creating a dynamic equilibrium such as $NH_3 + H_2O \rightleftharpoons NH_4^+ + OH^-$ that switches between local ionic and neutral arrangements, or as longer lived ionization events at low pressures, $NH_3 + H_2O \rightarrow NH_4^+ + OH^-$, which create ionic species seen in the high-pressure crystal structures. Alternatively, a different proton than the newly acquired proton hops to another neighbour, leading potentially to long-range diffusivity. This hopping mechanism, aided in nature by quantum tunneling (but not considered here), exists in low temperature ices already [52, 53], but with a very low diffusion rate.

A quantitative analysis of excitation events, e.g. comparing rotation and hopping rates, is complicated by proton transfer and thus local changes of molecular unit types, such as H_2O versus OH^- or H_3O^+. A qualitative description of what is observed in the different mixtures is given in table 1 for the case of AHH. Similar observations hold for all mixtures.
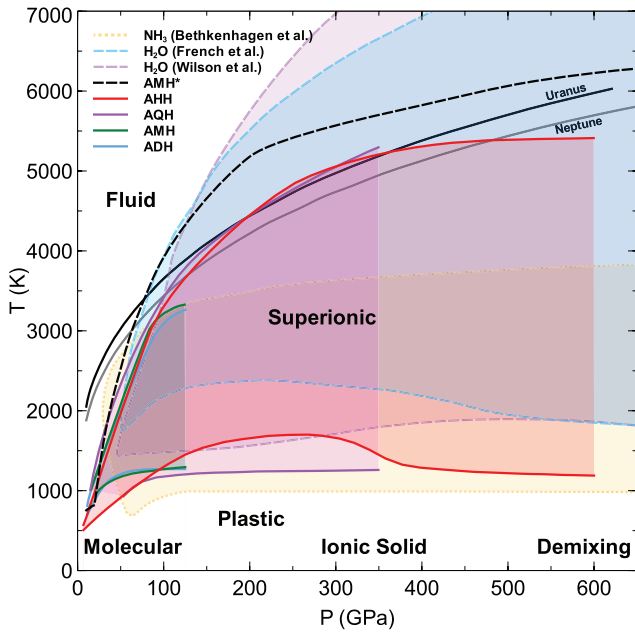
3.3. Superionicity and melting

In figure 5 we superimpose the superionic regimes of the different mixtures and add literature data for pure water and ammonia [54–56] as well as AMH [36]. Qualitatively, all ammonia–water mixtures behave similarly, which allows for the general labelling of regions in $P-T$ space, see figure 5: upon increasing pressure at low temperatures, molecular phases are superseded by ionic solids before eventual demixing; plastic phases are intermediaries upon heating before large regions of superionicity; and at high temperatures a molecular liquid transforms into an ionic liquid at high pressures. Both the onsets of superionicity and the melting lines of the mixtures are between the extrema of pure ammonia and water at pressures above 1 Mbar.

For water, Cavazzoni *et al* placed the solid–superionic–liquid triple point below 30 GPa, most likely around 20 GPa and 1200 K [16]. Hernandez *et al* place this triple point at 16 GPa and 810 K [42]. Differences exist due to the criterion used to designate superionicity and the grid of $P-T$ values chosen for simulations (which is much denser in [42]). For ammonia, Bethkenhagen *et al* report a solid–superionic–liquid triple point at roughly 25 GPa and 1200 K, from AIMD simulations that do not report any plastic phases [54]. Cavazzoni

Table 1. Summary of visual analysis of the dominant excitation events seen in AIMD of AHH at temperatures across the plastic regime.

P (GPa)	T (K)	Phase	Description
3	200	*I*	Rotations (NH_3)
3	400	*I*	Rotations (NH_3 and H_2O)
10	500	*II*	Rotation and ionization ($NH_3 + H_2O \rightarrow NH_4^+ + OH^-$)
10	750	*II*	Rotation and ionization
10	1000	*II*	Liquid
20	500	*II*	Rotation, ionization, exchange between O/N sites
20	1000	*II*	Superionic, exchange between O/N sites
20	1500	*II*	Liquid
40	1000	*A2/m*	Superionic along quasi-bcc diagonals
60	1000	*Amma*	Rotation and proton hopping ($NH_3 + H_2O \rightleftharpoons NH_4^+ + OH^-$)
100	1000	*Amma*	Rotation and proton hopping
350	1000	$P\bar{3}m1$	Rotation and proton hopping
400	1000	$P\bar{3}m1$	Rotation and proton hopping
500	1000	$P\bar{3}m1$	Rotation and proton hopping
500	1500	$P\bar{3}m1$	Superionic

et al show quite a different phase diagram with a plastic region above 600 K at 30 GPa and a solid–superionic–liquid triple point between 30 and 60 GPa and 1200 K [16]. For the mixtures, the solid-superionic-liquid triple points all lie below 30 GPa and 1000 K. For AHH the triple point appears around 10 GPa and 600 K, however, this is a plastic–superionic–liquid triple point unlike all others. Further simulations on finer grids around these triple points, similar to a recent study of water [42], would help identify exactly the type of these triple points and their locations. The AQH triple point is tentatively placed around 10 GPa and 900 K, though no actual AIMD melting simulations were performed below 10 GPa and the melting line is extrapolated below this pressure. For AMH the triple point occurs around 12 GPa and 850 K. For ADH the triple point lies around 12 GPa and 800 K though data suggests this

Figure 5. Superionic regions and melting lines for all four mixtures, with data for the individual ices taken from [54–56] and for AMH (labelled AMH*) from [36]. The highest pressure shown for each mixture corresponds to the AIMD $P - T$ region sampled and roughly corresponds to their limit of ground state stability.

could also be a plastic–superionic–liquid triple point. A much finer temperature grid was used for ADH up to 1000 K yet its triple point is found to be similar to the other mixtures. Mixing of ammonia and water can lead to enhanced proton transfer between different neutral and ionic molecular species, as witnessed in the plastic regime. This is likely the reason for the more moderate $P - T$ conditions to enter the superionic regime compared to water and ammonia individually.

In general, the mixtures have superionic regions that occupy mostly the same $P - T$ space. One obvious exception is the onset of superionicity in AHH, which is shifted to significantly higher temperatures between 150 and 350 GPa. This is likely due to the strong ionic bonding in the solid phases of this compound, with very stable $(NH_4^+)_2O^{2-}$ arrangements. A quantitative analysis of the superionic regions is presented later in this work.

The melting lines for all mixtures appear to closely follow those of ammonia and water individually up to about 100 GPa (see figure 5). Above 100 GPa ammonia melts at much lower temperatures than water. For example, at 300 GPa, ammonia is reported to melt around 3500 K compared to water at 6500 K. In this higher pressure region (above 1 Mbar), ammonia-water mixtures appear to melt directly in between the individual ices; for example, at 5000 K at 300 GPa. The calculated melting lines are also very close to the Uranus and Neptune isentropes, raising the possibility that the mixed planetary ices have a solid heavy atom lattice inside these planets above 2 Mbar.

Figure 5 also allows to compare the melting lines of the different mixtures with previous data on AMH and one another. On the resolution of the $P - T$ grid chosen, with temperature steps of 500 K above 1000 K the melting lines are very similar

above 50 GPa, rarely differing by more than 500 K. In comparison with data by Bethkenhagen *et al* [36] (labeled AMH* in figure 5), all melting lines determined in this work are at lower temperature, which likely indicates systematic differences in how the melting was determined, such as finite-size effects of the simulations and judging of melting by the MSD. Here, melting lines were calculated using a 'heat until it melts' method which has the shortcomings of super-heating and so is likely to over-estimate the melting temperature. Thus it can not be ruled out that ammonia–water mixtures are in a liquid state along the entire Neptune and Uranus isentropes. However, if these compounds are still able to form heavy atom alloys (such as DMA) at high $P - T$ conditions, these would benefit from additional configurational entropy that would increase the stability of alloyed superionic phases and push up the melt lines. Furthermore, an ammonia-rich alloyed phase may take a different ammonia:water ratio than 2:1 or 4:1 which could enhance the stability of solid and superionic phases further. As the melt lines are so close to the isentropes of Neptune and Uranus it would be of further interest to determine them more precisely above 50 GPa. This could include testing other simulation methods for melting transitions such as the Z-method, annealing, thermodynamic integration, and two-phase coexistence.

3.4. Local structure analyses

So far, the character of the different regimes (plastic, superionic, or liquid) has been determined using a combination of visual inspection and calculated MSD's for the different atom types. Already, this resulted in identifying a rich variety of behaviours: covalent bonds O–H and N–H can rotate, changing the hydrogen bond network; they can break, but only on a local scale (proton hopping) to create local ionic or molecular defects; or protons could be fully diffusive—with or without instantaneous attachment to a heavy atom. Here, we quantify these behaviours using a wider range of analysis tools. These will confirm our assignment of the different regions in the previous sections, and give additional insight into the microscopic character of the non-solid phases.

3.4.1. Radial and pair distribution functions. The radial distribution function (RDF) alone reveals information about the atomistic state of the simulated system, averaged over all constituents. For simple systems, this is sufficient to distinguish the solid and liquid phases, however, for a multi-component system additional complexity arises. A partial melt, as in the superionic phase, biases the RDF towards that of a typical liquid by losing much of the peak structure yet still retaining the peaks of the heavy atom sublattice. This is shown in the top panel of figure 6 for AHH at 100 GPa in the $P\bar{3}m1$ phase. By examining individual pair distribution functions (PDF) such as g_{NH}, g_{OH}, etc, more details about the system can be revealed.

The solid AHH-$P\bar{3}m1$ phase is ammonia-rich and consists of NH_4^+ and O^{2-} units. Hence, in the solid ($T = 500$ K) $g_{NH}(r)$ has a strong peak at the covalent distance $d_{NH} = 1.1$ Å, while $g_{OH}(r)$ has a first peak at the hydrogen-bonded distance
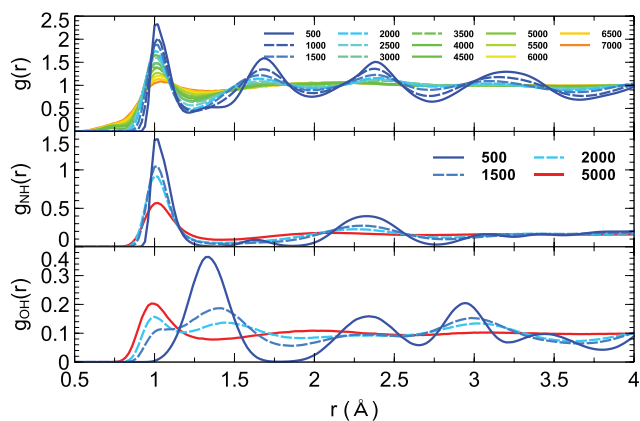
Figure 6. The RDF $g(r)$ (top panel) and PDF's $g_{NH}(r)$ and $g_{OH}(r)$ for AHH-$P\bar{3}m1$ at 100 GPa. Dashed lines indicate the superionic regime, which ranges from 1000–3500 K at this pressure.

Figure 7. PDF's for AHH-$P\bar{3}m1$ at 100 GPa. The dashed lines for $T = 2000$ K indicates a superionic phase. Labels indicate the likely chemistry where a peak emerges around a typical covalent bond length.

$d_{\mathrm{O\cdots HN}} = 1.3$ Å. The effect of heating into the superionic phase results in a gradual build-up of O–H covalent bonds, as a peak grows in $g_{OH}(r)$ at 1 Å (see figure 6). The hydrogen-bonded peak at 1.3 Å moves to larger distances and widens significantly with increased temperature; a consequence of both protons hopping across N–H $\cdots$ O but also of rotating NH$_3$ or NH$_4^+$ units. This peak only disappears in the molten phase, shown at 5000 K in figure 6. In fact, $g_{OH}(r)$ shows appreciable long-range order in the superionic phase, suggesting that while protons are diffusive they are not distributed homogeneously in the crystal. For $g_{NH}(r)$ on the other hand the covalent peak at 1 Å only broadens and reduces with temperature, demonstrating the unchanged nature of the N–H bond, and is only affected by protons hopping away from NH$_4^+$ units at high temperature. Even at 5000 K protons are most likely found in a covalent bond with either N or O; further down we will quantify this.

In the molten state, different PDF's shown in figure 7 reveal high pressure-high temperature chemistry. Firstly in $g_{HH}(r)$ a peak emerges at 4000 K around 0.75 Å, which is consistent with a typical H$_2$ bond length. However, pure hydrogen is atomic at this temperature and pressure, and the bond lifetime of these molecules is likely to be short, though the presence of the other constituents could encourage molecular H$_2$ to be present in these mixtures. This formation of H$_2$ also explains the growing shoulder at the lowest values of r in the full RDF $g(r)$, see figure 6. H$_2$ molecules appear only to form in the liquid, and not in the superionic phase. Furthermore, $g_{NN}(r)$ (see figure 7) shows the formation of N–N bonds peaked around 1.3 Å. These N–N bonds are longer than those found in static N$_2$ molecules (1.1 Å) but shorter than single N–N bonds in polymeric nitrogen (1.6 Å). These species are likely to be short-lived N$_2$ molecules in a highly rotating state or saturated N$_x$H$_y$ molecules. Lastly, there is a hint at the presence of N–O bonds, comparable in lengths to d_{NO} in nitric oxide (NO, 1.15 Å) or nitrogen dioxide (NO$_2$, 1.2 Å). The formation of O–O bonds (not shown) appears much more difficult in this compound. The full data set of RDF's and PDF's for all mixtures, pressures and temperatures simulated is
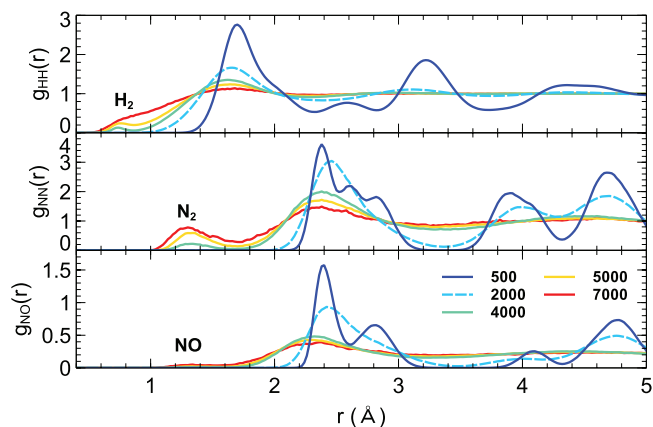
given in the supplementary information (SI) (stacks.iop.org/JPhysCM/32/184004/mmedia).

The fact these molecules appear to form at the same time in the molten state may be connected: the molten system allows for N, O ions to be free and become close enough to occasionally form covalent bonds. This means there are less covalent N–H and O–H bonds which allows the hydrogen atoms both space and the chemical freedom to form H$_2$ molecules. At higher temperatures still, the full dissociation of bonds is likely to occur on the way to a plasma. This can be seen for H$_2$ at 7000 K in figure 7 as the PDF $g_{HH}(r)$ forms a smooth and featureless distribution.

3.4.2. Chemical composition. The PDF analysis shows that various chemical species can be found in the mixtures. While this is most obvious in the fluid state, the proton mobility in the plastic and superionic phases allows for the co-existence of various species already at much lower temperatures—from the expected H$_2$O to the much rarer NH$_5^{2+}$, though specific abundances depend on the global stoichiometry. For example, ammonia-rich AHH and AQH are likely to feature O^{2-} units while in water-rich ADH these are much rarer. Here, we quantify the presence of particular molecular species by assigning protons to heavy atoms within a fixed cutoff radius. The local environment for each heavy atom (N,O) is screened and protons assigned up to a typical covalent bond length, chosen here as $r_c = 1.15$ Å. Counting the number of covalent bonds per (N,O) indicates whether the local molecular unit is, for example, NH$_2^-$ or NH$_4^+$, and thus we can track their presence as function of pressure, temperature, and composition. This may be sensitive to equilibration and run-time but simulations appear to find stable ratios quickly.

In figure 8 we show the fraction of the most relevant molecular species tracked in ADH and AHH, in each case normalized to the total of all heavy atoms, N and O. Other mixtures exhibit similar behaviour but depend also on the initial conditions, i.e. ground state structures. Overall the species present are dominated by the expected NH$_4^+$, NH$_3$, H$_2$O, OH$^-$, and O^{2-} units found in the ground state structures.
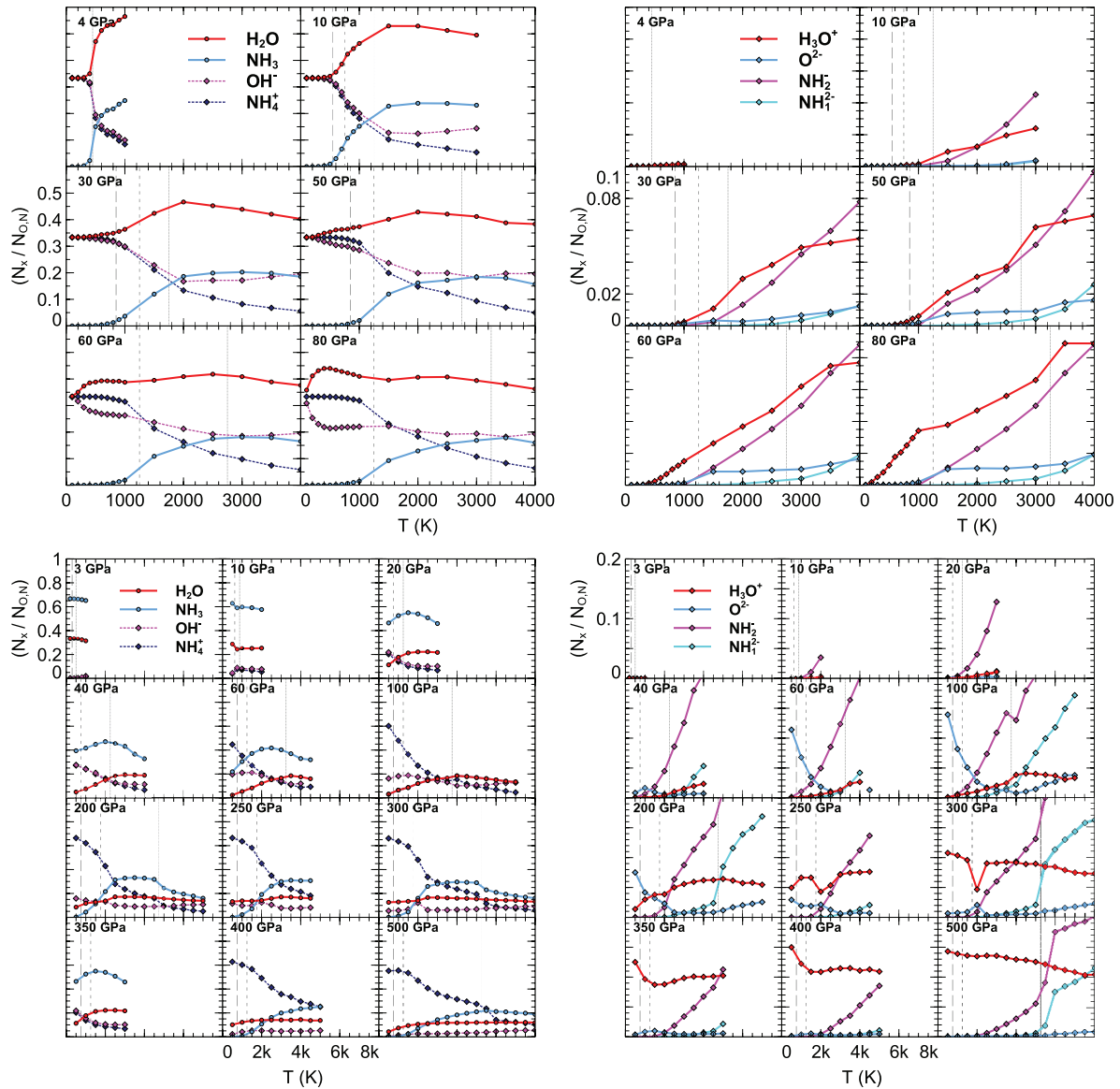
Figure 8. Relative abundance of most relevant species (left) and relatively rare chemical species (right) in simulations of ADH (top) and AHH (bottom).

Upon increasing temperature, the general trend is towards formation of neutral rather than ionic species. For example, high-pressure ammonia-rich hydrates with deprotonated oxygen O^{2-} have almost no species with O–H bonds (OH^- or H_2O) at low temperature, but their abundance increases as high-temperature regimes are entered. Conversely, the presence of ammonium, NH_4^+, is diminished at high temperature relative to ammonia, NH_3. In the case of ADH, with data on a fine temperature grid below 1000 K, the rise in NH_3 molecules mirrors the decrease in OH^- and NH_4^+ ionic species. This transition begins before full superionicity sets in, as consequence of proton transfer in the excited and plastic regions. In general, the chemical species follow these trends independent of global composition—though figure 8 shows the quantitative differences between ADH and AHH. The presence of rare units, such as H_3O^+ or NH_2^-, increases in likelihood once the superionic phases have been entered.

All ammonia hydrates under pressure benefit from proton transfer and the resultant formation of partially charged species to form ionic solids in the ground state. To quantify the temperature-induced changes to the partition into neutral (molecular) and charged (ionic) species we summarised the 'molecular' and 'ionic' species in the simulations. I.e. formally charged species such as NH_4^+ and OH^- are classed as ionic, whereas NH_3 and H_2O are molecular. The corresponding data for ADH is shown in figure 9, with data for other compositions given in the SI.

Note that the starting configurations in the ADH ground state structures always contain 2/3 ionic species. However, at all pressures we see a crossover from ionic dominance to molecular dominance on heating into the superionic phase, see figure 9. In the liquid, the molecular:ionic ratio is mostly independent of temperature, but shows some pressure dependence, with hot liquids becoming less molecular and more
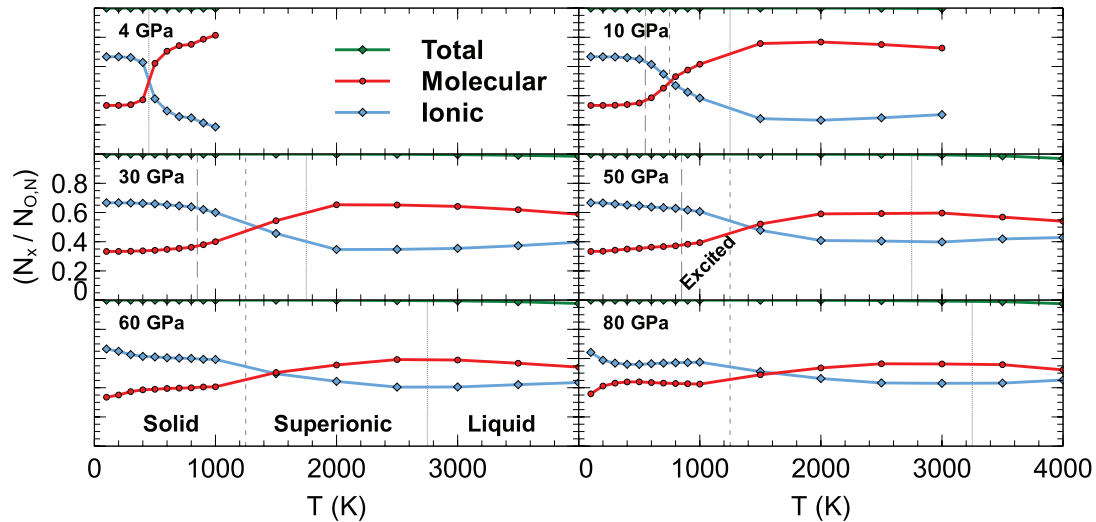
Figure 9. Analysis of molecular versus ionic species present in ADH as a function of *P* and *T*. Long/short dashed lines indicate the temperatures at which plastic/superionic phases were observed and dotted lines indicate the melting temperature.

ionic at higher pressures. For ammonia-rich hydrates AHH and AQH above 200 GPa only, the molecular:ionic ratio does not cross over in the superionic phase, instead converging to a stable equilibrium at high temperature possibly due to the increased number of protons and pressure heavily favoring ionic structures (see SI). Upon heating into the liquid state the total number of molecular and ionic units can fall slightly below 1.0 as a small number of protons in the simulations remains unaccounted for (and transient species such as N_2 form instead, see prior discussion).

By interpolating data on the molecular:ionic species ratio over the simulations' $P - T$ grids, phase diagrams can be produced for all hydrates that highlight the molecular content, as shown in figure 10. Across all mixtures, low temperatures favor ionic species as most high-pressure phases are essentially ionic structures. On heating, the molecular fraction rises, most clearly as mixtures enter the superionic regimes. Across the superionic phases the molecular content increases further yet becomes temperature independent in the liquid state, instead dependent on pressure. The highest temperatures see a return to more ionic features as more protons become entirely unbound, and in the 'warm dense matter' regime a full decomposition of all chemical species into individual ions would be expected. Overall, in these mixtures, molecular species are dominant at low pressures and high temperatures (both the superionic and the molecular liquid regime), whereas at high pressure and low or very high temperature ionic species dominate (either in solid or ionic liquid form).

3.4.3. Bond life times. To quantify the longevity of molecular species in our simulations we estimated the covalent N–H and O–H bond life times τ as given by the decay of the bond auto-correlation function $\beta(t)$ defined in eq. 1. A valid covalent bond $b_{ij}(t)$ is defined here by two conditions: by connecting a given proton i to the nearest heavy atom j (N or O) yet only within a radius $r_{ij} \leqslant 2.0$ Å. This means the number of covalent X–H bonds should be the same as the number of protons in the solid and superionic phase.

The results of this analysis for ADH are shown in figure 11 and for all other mixtures in the SI. At low temperatures bonds are found to be persistent and likely to survive into the future, and $\beta(t)$ is constant. As the BAC method measures the probability of protons to maintain contact to the closest nearest neighbour heavy atom, it captures information in systems with symmetric hydrogen bonds (N–H–N in AQH) or –(O–H)– chains (AMH, ADH). Their dynamics can be seen in figure 11 at 30–80 GPa for the O–H bonding at low temperature. There, $\beta_{O-H}(t)$ decreases with increasing temperature yet remains roughly constant over the simulation runs. This is because at those pressures 1/3 of the protons form O–H ⋯ O bonds and are in a double-well potential along the O–H–O connections present in the *Ama*2 and *P*2$_1$/*m* ADH structures. Protons hop between the two minima and in equilibrium this will uniformly reduce $\beta(t)$, by an amount that correlates to the hopping rate; the latter increases strongly with temperature. In the local excitation regime, molecular rotations should not influence $\beta(t)$, but proton hopping does, as it reduces a bond's life time. This is best seen in figure 11 for $\beta_{O-H}(t)$ at 10–50 GPa. Upon further heating into the superionic regime and the liquid state protons become fully mobile and $\beta(t)$ shows strongly temperature-dependent decay rates. Under all conditions, O–H bonds break more easily than N–H bonds, which reflects the propensity of these mixtures to form ionic solids with deprotonated water. But it also suggests that more of the superionic diffusion is mediated by the oxygen ions, which are more rapidly capturing and releasing protons moving through the lattice.

The exponentially decaying regime of the BAC has an associated life time τ_α, which is shown in figure 12 for all different mixtures. N–H bonds are more persistent than O–H bonds across the range of pressures and temperatures; at given $P - T$ conditions, τ_{N-H} is about 10 times larger than τ_{O-H}. The life times vary between 10s or 100s of picoseconds at low pressure and temperature (longer than the simulation runs) and 10s of femtoseconds at the highest pressures and temperatures. A sensible lower limit to declare a 'bond' could be that
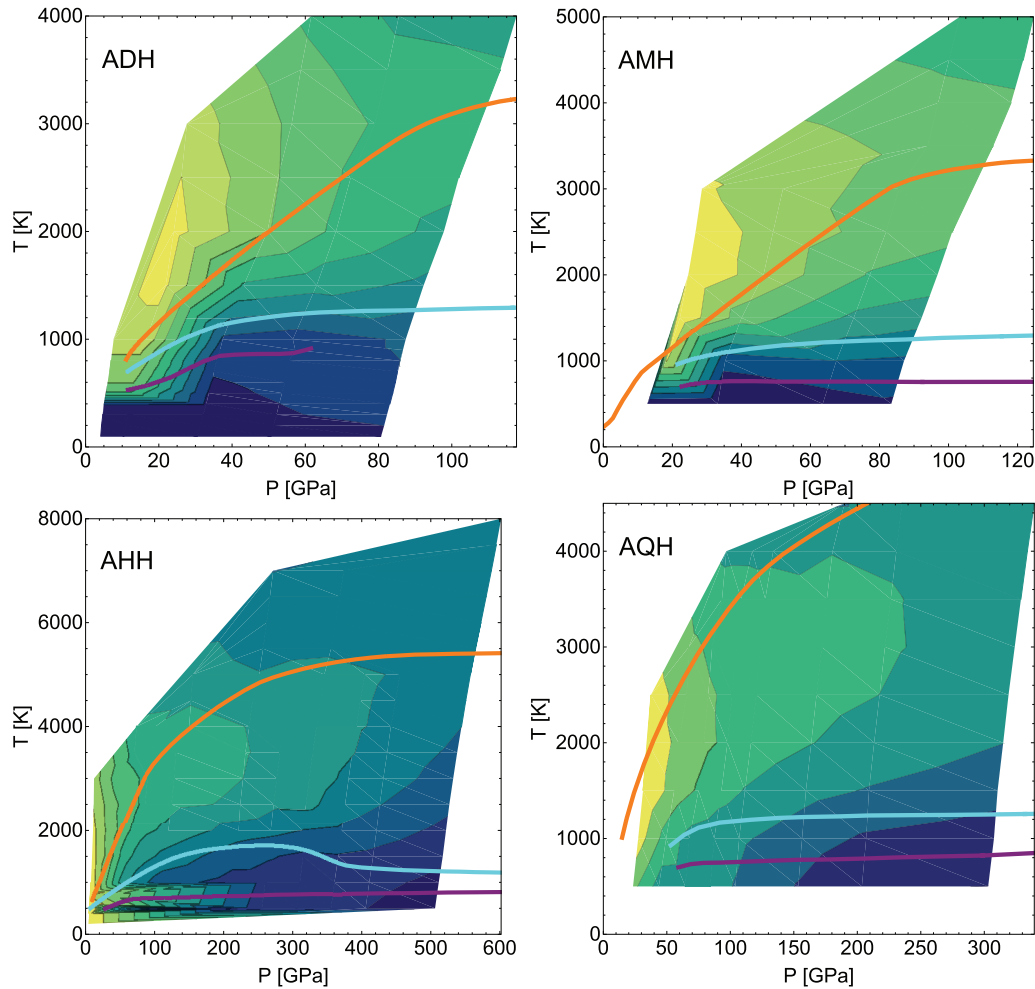
Figure 10. Fraction of molecular species found in ammonia–water mixtures, interpolated from 0.0 (dark blue) to 1.0 (yellow). From top left: ADH, AMH, AHH, and AQH. Orange/cyan/purple lines are the respective onsets of melt/superionic/plastic phases.

it should exist for a couple of vibrational periods which, for N–H and O–H vibrons in the 3000–4000 cm^{-1} range, equates to about 20 fs. In the superionic regime, bond life times interpolate smoothly between the solid and the fluid state, which implies that even though protons are diffusive, molecular units persist over finite periods of time; protons percolate through the heavy atom crystals and preferentially occupy molecular proton sites.

In some phases, a similar effect results in an *increase* of the bond life times upon entering the fluid phase, see e.g. AMH at 60-80 GPa and AQH at 60–100 GPa in figure 12. In those circumstances the fluid is more 'molecular' than the superionic regime with longer-lived chemical species. This correlates with a drop in the proton diffusion constant at the melting transition (see figure 2 and the SI) as protons in the molecular fluids are *less* mobile than in the superionic regime.

4. Conclusions

In summary, we report here the results of a systematic computational study of all known ammonia hydrates, using *ab initio* molecular dynamics at pressures and temperatures that replicate the conditions in the mantle regions of giant icy planets.

Considering a wide range of chemical compositions allows us to draw conclusions that we expect to hold for arbitrary mixing ratios of these two planetary ices.

Upon heating, all ammonia–water mixtures exhibit similar phase transitions as those found in the individual ices of ammonia and water. Specifically, in the low pressure region solid phases melt fully and directly enter a molecular liquid regime. At moderate pressures above 10 GPa a plastic or locally excited regime is found in all four mixtures, which had not been considered in previous studies. The plastic phases show different local motifs than in the individual ices, due to the chemical complexity present in the mixtures—e.g. proton hopping and therefore a dynamical equilibrium between ionic and neutral species. Further heating results in superionic behaviour with fast diffusing protons in all mixtures. The superionic regimes cover large areas of $P - T$ space, with solid–liquid–superionic triple points at relatively low pressures and temperatures. We attribute the relatively moderate conditions required to enter the superionic states to the chemical complexity of the mixtures that allows different routes to induce protons hopping between lattice sites. Melting lines were obtained by simple direct heating and were shown to be very close to the isentropes of Uranus and Neptune and
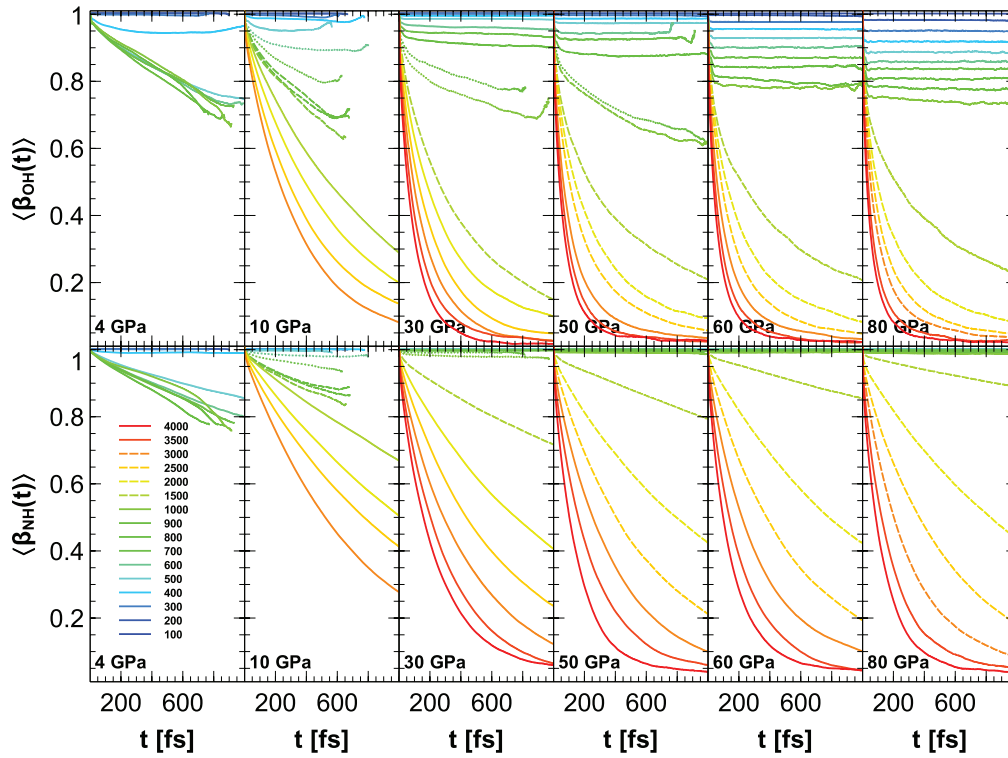
Figure 11. Bond auto correlation functions $\beta(t)$ for O–H (top) and N–H bonds (bottom) in ADH. Dashed lines refer to the superionic regime and dotted lines refer to the excited or plastic regime.
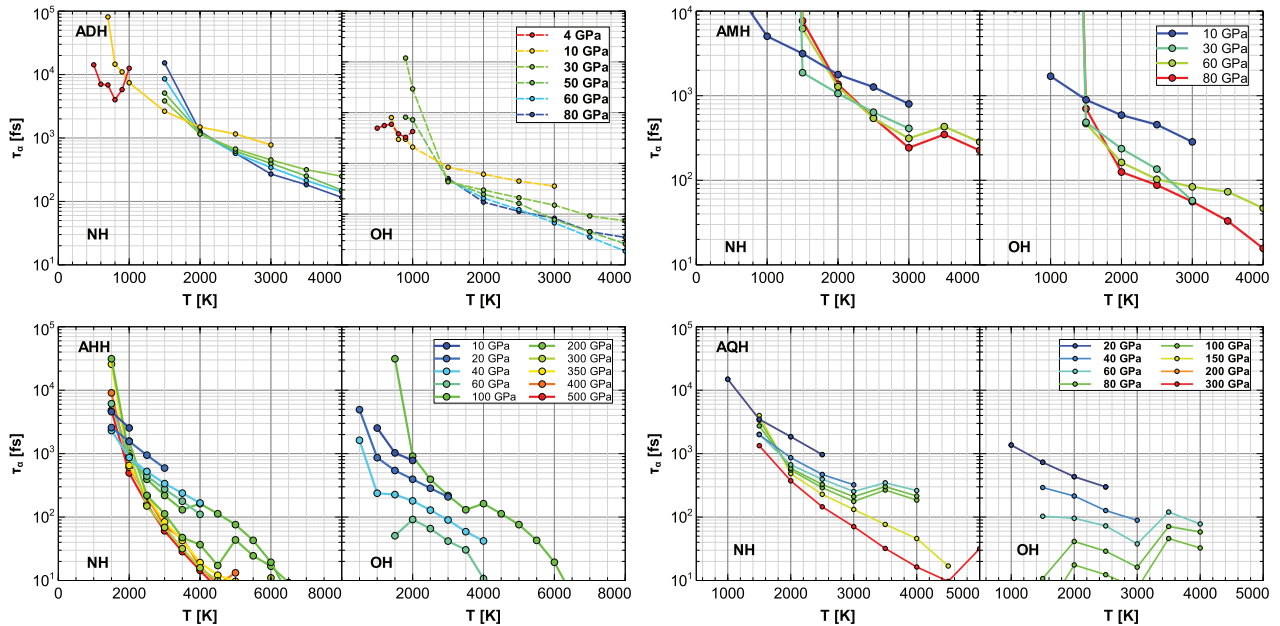
Figure 12. From top left: bond life times τ estimated from the BAC's $\beta_{NH}(t)$ and $\beta_{OH}(t)$ for ADH, AMH, AHH, and AQH as function of temperatures and for a range of pressures. For each mixture, the left panel shows τ_{NH}, the right panel shows τ_{OH}.

located between those of separate ammonia and water ices. Interestingly the four mixtures' melting lines are very close in $P - T$ space.

In comparison to previous simulations of ADH and AMH, we produced qualitatively similar results, though this work considered more relevant high-pressure solid phases and usually larger simulation cells. As a consequence, we could identify the locally excited plastic regime in the mixtures (which must not be mistaken for superionicity in analyses of short MD runs) and obtain melting lines that are generally lower than those reported in the literature. Our results suggest that this can make a qualitative difference for the lower

mantles of the ice giants, where simulations are not fully conclusive on whether liquid or superionic (solid) phases should be present.

Local structure analyses of the different high-temperature regimes showed that heating generally favours neutral over ionic molecular species. We also find that the superionic regime is dominated by short-lived molecules. The diffusive protons therefore do not move freely through the crystal but occupy molecular sites at virtually all times. The life times of these species decreases continuously with increases in temperature, with N–H bonds longer lived (and therefore 'stronger') than O–H bonds.

For some mixtures and specific $P - T$ conditions, the melting transition coincides with a drop in proton diffusivity. There, counterintuitively, heating from a solid (superionic) into a liquid phase *reduces* the mobility of the particles involved. This phenomenon is restricted to $P - T$ conditions where the fluid phase is best characterised as a molecular liquid, and proton diffusivity is limited by the mobility of the molecular species. The highest combined $P - T$ conditions favour the formation of ionic liquids.

Our study provides another step towards more realistic modelling of the interiors of icy planets. By screening a wide range of chemical composition we could extract characteristics that are common across a wide range of mixtures (the occurrence of plastic and superionic phases, trends in the chemical composition) and others that require more attention in future work—e.g. precise validations of the melting lines through different simulation methodology, or conductive and transport properties of the non-solid phases. Yet more work is required to understand the role of other species such as methane or hydrogen as ingredients of more complex mixtures, or the solubility of heavy core elements at the base of the planets' mantle regions.

Acknowledgments

ORCID iDs

Victor Naden Robinson https://orcid.org/0000-0002-9198-9154
Andreas Hermann https://orcid.org/0000-0002-8971-3933

References

[1] Hubbard W B and MacFarlane J J 1980 Structure and evolution of Uranus and Neptune *J. Geophys. Res.* **85** 225–34

[2] Ross M 1981 The ice layer in Uranus and Neptune diamonds in the sky? *Nature* **292** 435–6

[3] Young L A *et al* 2008 New horizons: anticipated scientific investigations at the Pluto system *Space Sci. Rev.* **140** 93–127

[4] Sekine Y, Genda H, Sugita S, Kadono T and Matsui T 2011 Replacement and late formation of atmospheric N_2 on undifferentiated Titan by impacts *Nature Geosci.* **4** 359–62

[5] Sotin C, Grasset O and Mocquet A 2007 Mass–radius curve for extrasolar Earth-like planets and ocean planets *Icarus* **191** 337–51

[6] Rauer H *et al* 2014 The PLATO 2.0 mission *Exp. Astron.* **38** 249–330

[7] Noack L, Snellen I and Rauer H 2017 Water in extrasolar planets and implications for habitability *Space Sci. Rev.* **212** 877–98

[8] Podolak M, Weizman A and Marley M 1995 Comparative models of Uranus and Neptune *Planet. Space Sci.* **43** 1517–22

[9] Nettelmann N, Wang K, Fortney J J, Hamel S, Yellamilli S, Bethkenhagen M and Redmer R 2016 Uranus evolution models with simple thermal boundary layers *Icarus* **275** 107–16

[10] Zhang W, Oganov A R, Goncharov A F, Zhu Q, Boulfelfel S E, Lyakhov A O, Stavrou E, Somayazulu M, Prakapenka V B and Konôpková Z 2013 Unexpected stable stoichiometries of sodium chlorides *Science* **342** 1502–5

[11] Zhu L, Liu H, Pickard C J, Zou G and Ma Y 2014 Reactions of xenon with iron and nickel are predicted in the Earth's inner core *Nat. Chem.* **6** 644–8

[12] Hermann A and Schwerdtfeger P 2014 Xenon suboxides stable under pressure *J. Phys. Chem. Lett.* **5** 4336–42

[13] Lobanov S S, Prakapenka V B, Prescher C, Konôpkova Z, Liermann H-P, Crispin K, Zhang C and Goncharov A F 2015 Pressure, stress, and strain distribution in the double-stage diamond anvil cell *J. Appl. Phys.* **118** 035905

[14] Hermann A 2017 Chemical bonding at high pressure *Reviews in Computational Chemistry* ed A L Parrill and K B Lipkowitz (New York: Wiley) pp 1–41

[15] Benedetti L R, Nguyen J H, Caldwell W A, Liu H, Kruger M and Jeanloz R 1999 Dissociation of CH_4 at high pressures and temperatures: diamond formation in giant planet interiors? *Science* **286** 100–2

[16] Cavazzoni C, Chiarotti G L, Scandolo S, Tosatti E, Bernasconi M and Parrinello M 1999 Superionic and metallic states of water and Ammonia at giant planet conditions *Science* **283** 44–6

[17] Wang Y, Liu H, Lv J, Zhu L, Wang H and Ma Y 2011 High pressure partially ionic phase of water ice *Nat. Commun.* **2** 563

[18] Hermann A, Ashcroft N W and Hoffmann R 2012 High pressure ices *Proc. Natl Acad. Sci. USA* **109** 745–50

[19] Pickard C J, Martinez-Canales M and Needs R J 2013 Decomposition and terapascal phases of water ice *Phys. Rev. Lett.* **110** 245701

[20] Palasyuk T *et al* 2014 Ammonia as a case study for the spontaneous ionization of a simple hydrogen-bonded compound *Nat. Commun.* **5** 3460

[21] Ninet S, Datchi F, Dumas P, Mezouar M, Garbarino G, Mafety A, Pickard C J, Needs R J and Saitta A M 2014

Experimental and theoretical evidence for an ionic crystal of ammonia at high pressure *Phys. Rev.* B **89** 174103

[22] Pruteanu C G, Ackland G J, Poon W C K and Loveday J S 2017 When immiscible becomes miscible-methane in water at high pressures *Sci. Adv.* **3** e1700240

[23] Liu C *et al* 2017 Topologically frustrated ionisation in a water-ammonia ice mixture *Nat. Commun.* **8** 1065

[24] Naden Robinson V, Wang Y, Ma Y and Hermann A 2017 Stabilization of ammonia-rich hydrate inside icy planets *Proc. Natl Acad. Sci.* **114** 9003–8

[25] Naden Robinson V, Marqués M, Wang Y, Ma Y and Hermann A 2018 Novel phases in ammonia–water mixtures under pressure *J. Chem. Phys.* **149** 234501

[26] Conway L J and Hermann A 2019 High pressure hydrocarbons revisited: from van der Waals compounds to diamond *Geosciences* **9** 227

[27] Loveday J S and Nelmes R J 2004 The ammonia hydrates model mixed-hydrogen-bonded systems *High Press. Res.* **24** 45–55

[28] Fortes A D and Choukroun M 2010 Phase behaviour of ices and hydrates *Space Sci. Rev.* **153** 185–218

[29] Asplund M, Grevesse N, Sauval A J and Scott P 2009 The chemical composition of the sun *Annu. Rev. Astron. Astrophys.* **47** 481–522

[30] Fortes A D, Wood I G, Alfredsson M, Vočadlo L, Knight K S, Marshall W, Tucker M and Fernandez-Alonso F 2007 The high-pressure phase diagram of ammonia dihydrate *High Press. Res.* **27** 201–12

[31] Wilson C W, Bull C L, Stinton G and Loveday J S 2012 Pressure-induced dehydration and the structure of ammonia hemihydrate-ii *J. Chem. Phys.* **136** 094506

[32] Loveday J and Nelmes R 1999 Ammonia monohydrate VI: a Hydrogen-bonded molecular alloy *Phys. Rev. Lett.* **83** 4329

[33] Loveday J S, Nelmes R J, Bull C L, Maynard-Casely H E and Guthrie M 2009 Observation of ammonia dihydrate in the AMH-VI structure at room temperature possible implications for the outer solar system *High Press. Res.* **29** 396–404

[34] Wilson C, Bull C, Stinton G, Amos D, Donnelly M-E and Loveday J 2015 On the stability of the disordered molecular alloy phase of Ammonia hemihydrate *J. Chem. Phys.* **142** 094707

[35] Ma C, Li F, Zhou Q, Huang F, Wang J, Zhang M, Wang Z and Cui Q 2012 Ammonia molecule rotation of pressure-induced phase transition in Ammonia hemihydrates 2nh 3· h 2 o *RSC Advances* **2** 4920–4

[36] Bethkenhagen M, Cebulla D, Redmer R and Hamel S 2015 Superionic phases of the 1:1 water–ammonia mixture *J. Phys. Chem.* A **119** 10582–8

[37] Jiang X, Wu X, Zheng Z, Huang Y, Zhao J and Information S 2017 Ionic and superionic phases in ammonia dihydrate NH_3 $2H_2O$ under high pressure *Phys. Rev.* B **95** 144104

[38] Boyce J B and Huberman B A 1979 Superionic conductors: transitions, structures, dynamics *Phys. Rep.* **51** 189–265

[39] Takii Y, Koga K and Tanaka H 2008 A plastic phase of water from computer simulation *J. Chem. Phys.* **128** 204501

[40] Aragones J and Vega C 2009 Plastic crystal phases of simple water models *J. Chem. Phys.* **130** 244504

[41] Ninet S, Datchi F and Saitta A 2012 Proton disorder and superionicity in hot dense ammonia ice *Phys. Rev. Lett.* **108** 165702

[42] Hernandez J-A and Caracas R 2018 Proton dynamics and the phase diagram of dense water ice *J. Chem. Phys.* **148** 214501

[43] Chau R, Mitchell A C, Minich R W and Nellis W J 2001 Electrical conductivity of water compressed dynamically to pressures of 70–180 GPa (0.7–1.8 Mbar) *J. Chem. Phys.* **114** 1361–5

[44] Ojwang J G O, McWilliams R S, Ke X and Goncharov A F 2012 Melting and dissociation of ammonia at high pressure and high temperature *J. Chem. Phys.* **137** 064507

[45] Millot M, Hamel S, Rygg J R, Celliers P M, Collins G W, Coppari F, Fratanduono D E, Jeanloz R, Swift D C and Eggert J H 2018 Experimental evidence for superionic water ice using shock compression *Nat. Phys.* **14** 297–302

[46] Millot M, Coppari F, Rygg J R, Correa Barrios A, Hamel S, Swift D C and Eggert J H 2019 Nanosecond X-ray diffraction of shock-compressed superionic water ice *Nature* **569** 251–5

[47] Liu C, Gao H, Wang Y, Needs R J, Pickard C J, Sun J, Wang H-T and Xing D 2019 Multiple superionic states in helium-water compounds *Nat. Phys.* **15** 1065–70

[48] Bethkenhagen M *et al* 2017 Planetary ices and the linear mixing approximation *Astrophys. J.* **848** 67

[49] Segall M, Lindan P J, Probert M A, Pickard C, Hasnip P, Clark S and Payne M 2002 First-principles simulation: ideas, illustrations and the CASTEP code *J. Phys.: Condens. Matter* **14** 2717

[50] Hammer B, Hansen L B and Nørskov J K 1999 Improved adsorption energetics within density-functional theory using revised Perdew–Burke–Ernzerhof functionals *Phys. Rev.* B **59** 7413

[51] Redmer R, Mattsson T R, Nettelmann N and French M 2011 The phase diagram of water and the magnetic fields of Uranus and Neptune *Icarus* **211** 798–803

[52] Marx D, Tuckerman M E, Hutter J and Parrinello M 1999 The nature of the Hydrated excess proton in water *Nature* **397** 601

[53] Marx D 2006 Proton transfer 200 years after {von Grotthuss}: insights from *ab initio* simulations *ChemPhysChem* **7** 1848

[54] Bethkenhagen M, French M and Redmer R 2013 Equation of state and phase diagram of ammonia at high pressures from *ab initio* simulations *J. Chem. Phys.* **138** 234504

[55] French M, Mattsson T R, Nettelmann N and Redmer R 2009 Equation of state and phase diagram of water at ultrahigh pressures as in planetary interiors *Phys. Rev.* B **79** 054107

[56] Wilson H F, Wong M L and Militzer B 2013 Superionic to superionic phase change in water: consequences for the interiors of Uranus and Neptune *Phys. Rev. Lett.* **110** 151102